Load current control of one pulse width modulation for dynamic wireless power transfer system using vehicular ac current estimation

Toshiyuki Fujita, *Member, IEEE*, and Hiroshi Fujimoto, *Member, IEEE*,

Abstract—A wireless power transfer (WPT) system has been considered applicable to various charging applications. Dynamic WPT technology for EVs limits communication speed and capacity due to the separation of assemblies between the ground and vehicle sides. It is challenging to communicate signals synchronized with the transmission frequency at the same timing. Hence, the system that controls the power only by the vehicle itself is necessary for the sake of safety. This paper proposes a dynamic WPT system in which only the vehicle-side assembly acquires a synchronized signal and controls the load current to the battery. The theoretical analysis concludes that an input voltage derives an output ac current as a constant, and the one-pulse-width modulation for a converter changes a load current. A feed-forward control method of its current estimation is proposed. The bench system is designed, constructed, and tested to verify the effectiveness of the proposed method compared with the proportional-integral control in a static state. Furthermore, the system is also verified when in motion. The load current was limited to the maximum value of the system in areas where the coupling coefficient is high, while the current value was well controlled in the other areas.

Index Terms—Inductive power transfer, synchronous rectification, pulse width modulation, current estimation, feed forward control

I. INTRODUCTION

Electric Vehicles (EVs) have attracted attention for its excellent environmental performances. What is more, Wireless Power Transfer (WPT) technology has been developed [1], [2] and manufactured as an integral component of apparatus in home appliances, consumer products, drone [3], autonomous underwater vehicle [4] and industrial application [5] where there is a high demand for an ease of driver's usability and safety when charging. WPT technology based on magnetic resonance introduced [6] is highly efficient and tolerant to positional coupling even at distances of several ten centimeters to several meters, so it is anticipated that WPT technology will be developed not only for the sake of EV use in the stationary (static) WPT system, but also in motion (dynamic) system.

WPT technology is a solution without trade-off for a short mileage and a long charging time which is indispensable of EVs. Nevertheless, Dynamic WPT (DWPT) system has

T. Fujita, H. Fujimoto are with Graduate School of Frontier Sciences, the University of Tokyo, 5-1-5, Kashiwanoha, Kashiwa City, Chiba, 277-8561, Japan (e-mail: t-fujita@edu.k.u-tokyo.ac.jp)

been examined by diverse research groups [7]–[12]. When making a DWPT system practical, there are various issues to be solved. As the coupling coefficient changes dramatically during driving state, this approach suggest both the coil arrangement and the circuit topology to make the output power constant [10]. The transmitter coils need to be embedded in the ground for the EVs to drive, and the impact of burial and packaging with concrete is being examined [11]. In addition, a new inverter topology is proposed to reduce the installation number of inverters [12].

Since the power receiving coil is moving in DWPT system, the time spent on a single transmitter coil is limited. Therefore, signal communication between the transmitter and receiver coils is small in volume. Consequently, it is desirable to acquire synchronization signals and estimable information without transmission as much as possible, for they lead to the problem of latency. The latency of communication is in the order of milliseconds [13], which is several orders of magnitude greater than the operating frequency of a WPT system. Hence, some studies are developed in estimation method. The coupling coefficient and mutual inductance are estimated by changing the transmitter dc voltage and measuring the current transient response [14]. The system adopts an additional vehicle coil and uses the voltage of the coil as a synchronous signal [15]. Our research group has also presented on a synchronous rectification and propose a system to obtain a synchronization signal from the voltage of the vehicle-side resonant capacitor [16].

Various research have been conducted to control the state of a WPT system by using an active rectifier on the vehicle side. An article reports on the improvement of efficiency in the case of misalignment by using a semibridgeless active rectifier as a pulse width modulation (PWM) based control to adjust the impedance of the power receiving side [17]. A system also controls the resonance condition on the receiver (vehicle) side by adding some phases of the receiver ac current and voltage to maximize efficiency [15]. A Model predictive control (MPC) allows the dc/dc converter to run at a higher speed than the proportional-integral-differential (PID) control, and its converter is installed at the output of the WPT diode rectifier [18]. The PID control uses the input voltage of the converter as a control parameter. Furthermore, the control parameters of MPC are the input/output voltage and inductor current of the converter. All of these parameters can be obtained independently by the vehicle. The operation of the systems is based on the exchange of information between
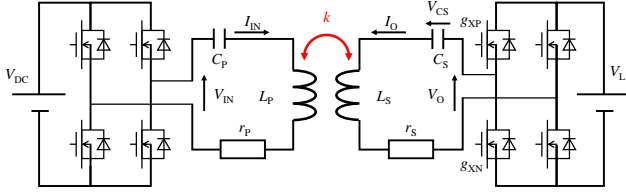
Fig. 1: Concept of the proposed wireless power transfer system.

Fig. 2: Equivalent circuit to the SS topology WPT system.

the transmitter and receiver, and wireless communication is essential for these systems. Much information exchange leads to bandwidth compression, so the system should be simple and based on safety.

This paper proposes the load current control method for a DWPT system only using vehicle-side assemblies when the suppression of the current is needed due to vehicle condition. The DWPT system presented here is designed to have a distributed arrangement of ground-side coils, which are long in the direction of vehicle travel. In addition, a full-bridge SiC converter is used for the vehicle-side rectifier (converter) to control the current on the vehicle side. One PWM control is used for current control which carrier frequency is the same as the load current to be regulated. Moreover, the synchronous signal is sensed by the resonant capacitor voltage on the vehicle side [16]. The current control consists of estimating the vehicle-side coil ac current and using a feed forward (FF) control from the estimated ac value. In section 2, the characteristics of the WPT circuit and the proposed PWM control with a delay of a phase for a circuit component and a change of pulse width due to a dead time are analyzed with the description of the proposed current estimation method. Section 3 compares the effectiveness of the proposed method with PI control in a stationary state. Furthermore, the experimental results are presented for a running state where the coupling coefficient changes while moving, and it is confirmed that the current is controlled to be stable by the proposed method.

II. THEORETICAL ANALYSIS AND CONTROL METHOD

A. Main Circuit Configuration

Fig. 1 shows the circuit configuration of a WPT system in this experiment, which is based on the so-called "series-series" WPT system [19]. A voltage-controlled power-factor-correction (PFC) circuit or ac/dc converter is connected to 200 V, 50 Hz ac mains. This part is not shown in Fig. 1. A full-bridge inverter operating at a high frequency of 85 kHz is used for the proposed WPT system. The switching devices used in the inverter are SiC MOSFETs. The primary coil and the secondary coil are connected in series with the primary resonant capacitor C_P and the secondary resonant capacitor C_S, respectively. A single-phase full-bridge converter (active rectifier) is used to achieve ac-to-dc power conversion at the receiving end. The devices are also used for SiC MOSFETs. A constant voltage load is used instead of a battery as the load. Furthermore, as shown in Fig. 1, the positive directions of each voltage and current are defined, respectively.
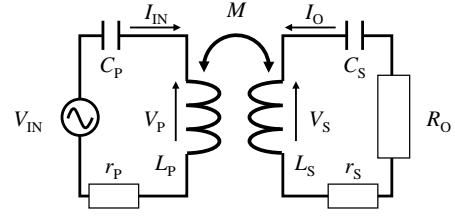
B. WPT Circuit Analysis

Fig. 2 shows an equivalent circuit of the WPT system at a fundamental frequency of 85 kHz in Fig. 1. The input voltage and angular frequency are represented as V_{IN} and ω, assuming a sinusoidal voltage. The self inductances of the primary coil and the secondary coil are defined as L_P and L_S, respectively. The mutual inductance between the primary and secondary coils is defined as M. The winding resistances r_P, r_S take account of skin effect and proximity effect and the equivalent ferrite-core-loss resistance. After the analysis, these resistances are eliminated from the following analysis. The coupling coefficient k of the WPT coils is defined using L_P, L_S, M;

$$k = \frac{M}{\sqrt{L_P L_S}}. \tag{1}$$

The current and voltage directions are defined as shown in Fig. 2. The back electromotive forces V_P and V_S are given by a function of the primary and secondary coil currents I_{IN} and I_O as follows;

$$V_P = j\omega L_P I_{IN} + j\omega M I_O. \tag{2}$$
$$V_S = j\omega M I_{IN} + j\omega L_S I_O. \tag{3}$$

The primary and secondary circuits give

$$V_{IN} = V_P + \frac{I_{IN}}{j\omega C_P}. \tag{4}$$

$$V_O = \frac{I_O}{j\omega C_S} + V_S. \tag{5}$$

To achieve effective power transfer, the power factors at input and output voltage and current approximates unity in Eqs. (4) and (5). Two resonant capacitors are determined from Eq. (6) [19].

$$\omega = \frac{1}{\sqrt{C_P L_P}} = \frac{1}{\sqrt{C_S L_S}}. \tag{6}$$

Substituting (6) into (4) and (5), the input and output voltage are calculated as

$$V_{IN} = j\omega M I_O. \tag{7}$$
$$V_O = j\omega M I_{IN}. \tag{8}$$

Eq. (7) indicates that the output current I_O is proportional to input voltage V_{IN}. The input inpedance Z_{IN} is also calculated using Eqs. (7) and (8) as

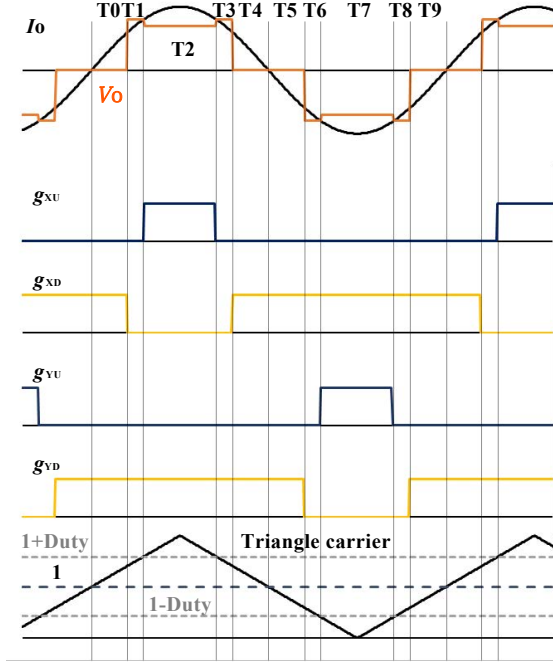$$Z_{IN} = \frac{\omega^2 M^2}{R_O}. \tag{9}$$

Fig. 3: Schematic state at a specific time of the proposed PWM control method. The uppermost graph is the relationship between the output current and voltage, and the middle four graphs are the gate signals of each converter device, which gates shown in Fig. 1. The lower graph is the triangular waveforms of PWM control used to generate the gate signals.
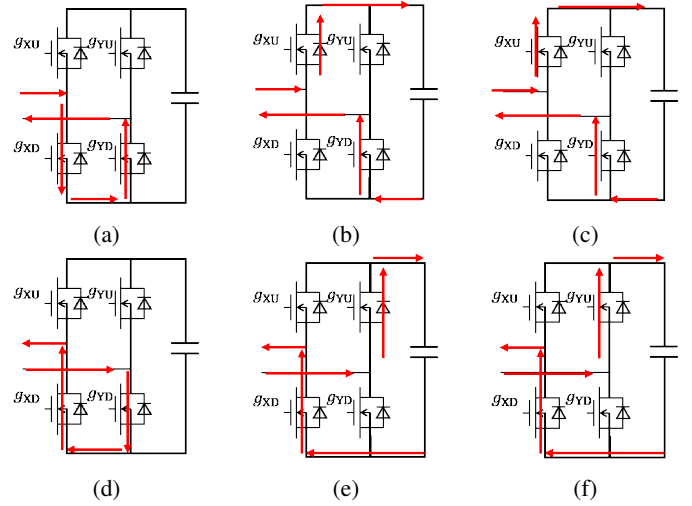

Fig. 4: Current paths through the device during one cycle based on the triangular wave comparison with the period of the switch timing shown in Fig. 3 implemented in this experiments. (a) Current path during the periods of T0 and T4. (b) Path of T1 and T3. (c) Path of T2. (d) Path of T5 and T9. (e) Path of T6 and T8. (f) Path of T7.

Further study is also conducted on efficiency and circuit characteristics, including parasitic resistance of the WPT coils [20].

Input voltage V_{IN} in Fig. 1 is designed to be a square wave or three-level wave input throughout this paper. V_{IN} comprises not only the fundamental wave, 85 kHz, but also harmonic components. When a frequency of a harmonic input voltage is $n\omega$ and other parameters are the same as fundamental wave condition, the input impedance, when calculated as in the derivation of Eq. (9), can be written as follows:

$$Z_{\text{IN}n\omega} = \frac{n^2\omega^2 M^2}{R_{\text{O}}^2 + \{(n^2-1)/n\}^2\omega^2 L_{\text{S}}^2} R_{\text{O}} \qquad (10)$$
$$+j\frac{n^2-1}{n}\omega L_{\text{P}}\left\{1 - \frac{n^2\omega^2 k^2}{\frac{R_{\text{O}}^2}{L_{\text{S}}^2} + \frac{(n^2-1)^2}{n^2}\omega^2}\right\}.$$

If n=3, the absolute value of Eq. (10) is 43.87 times larger than the fundamental impedance Z_{IN} at static condition of this experimental setup. Based on this calculation, the harmonic output current of Eq. (6) is negligible because the input impedance is large. Thus, output current I_{O} can be obtained a sinusoidal wave in the case of Fig. 1.

C. One pulse width modulation control

Fig. 3 illustrates the switching pattern based on the triangular wave comparison method proposed and implemented in this paper. This is because the gate waveform can easily be generated from the duty command value as shown in Fig. 3. The proposed method uses the vehicle-side resonant capacitor voltage V_{CS} as the synchronization signal. V_{CS} is used because the voltage detection method has fewer errors and delays than the current sensor for a circuit board, the voltage sensor can be implemented in a small circuit area, and the FPGA program for synchronizing the triangular wave carrier is easy to be programmed [16]. V_{CS} can be described using I_{O} as follows.

$$V_{\text{CS}} = \frac{I_{\text{O}}}{j\omega C_{\text{S}}}. \qquad (11)$$

As shown in Eq. (11), the triangular wave carrier shown in Fig. 3 can be synchronized with the current by setting the carrier to zero at the rising edge of the zero-crossing V_{CS} when the capacitor voltage goes from positive to negative. Further discussion is displayed in [16]. By inputting gate signals to the upper and lower arms, a desirable waveform with controlled various width can be obtained, but the presence of a dead time provides a voltage with a wider width than the duty input signal at this situation. The bottom figure of Fig. 3 also shows the waveforms of the triangular wave comparison method implemented in this paper. The zero-crossing signal of the vehicle-side resonant capacitor voltage is used as the synchronization signal. When the capacitor voltage rises zero-crossing point from minus value, the triangle carrier resets to zero, and count up as shown in Fig. 3. The frequency is calculated by the digital phase lock loop of the FPGA implementation, which generates a triangle wave of height 2 with the same frequency and phase as the vehicle-side capacitor signal. The comparison between the triangular wave and a dashed line of height one displayed in Fig. 3 generates a square wave, which is equivalent to synchronous rectification. The duty is defined as d $(0 < d < 1)$ for pulse width control. The comparison is the same as that of synchronous way with
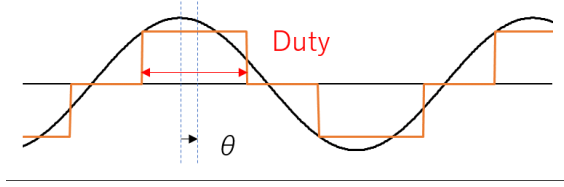
Fig. 5: Current and voltage waveforms of I_O and V_O with PWM in phase.

the difference of the line height being $1 + d$. This comparison generates the gate signal for X-side arm. The Y-side compares with $1 - d$ to generate gate signals for g_{YU}, g_{YD} illustrated in Fig. 3.

Fig. 4 describes the current pass of the converter which corresponds the switching state $TN(N \in \mathbb{R})$ shown in Fig. 3. The red arrows in Fig. 4 indicate the direction of the flowing current. Note that Fig. 1 does not show the polarity of the currents, but rather the actual positive current flow. Fig. 4a shows the circuit state of T0 shown in Fig. 3 which passes through the MOSFET of upper X side (hereafter XU MOS) and then through YD MOS back to the vehicle-side coil. Therefore, the output voltage V_O is zero. Fig. 4b shows the state of T1 in Fig. 3. When X-side arm is in a dead time, the current pass of the device depends on the direction of the current, and the state T1 passes through the XU body diode as shown in Fig. 4b. Thus, the voltage V_O is the sum of the load voltage and the diode voltage. Fig. 4c shows the state of T2 in Fig. 3. By T2, V_O is the load voltage, passing through the XU and YD MOSs. T3 behaves same as T1. T4 is identical to that of T0. Fig. 4d shows the current pass of T5 in Fig. 3. At T5, the current direction is reversed, so the circumstance of devices is in the same state as at T0 and T5. Since V_O remains zero. Fig. 4e shows the state of T6 in Fig. 3. At T6, the Y-side arm has a dead time and goes through the YU body diode. Just as in T1 and T3, V_O is a negative sum of the diode voltage and the load voltage. Fig. 4f shows the current pass of T6 in Fig. 3. T7 is the same as T2, but the only difference is a negative value of the load voltage. T8 has the same result as T6. In addition, T9 follows the same path as T5.

Fig. 5 shows the ideal current and voltage waveforms of the converter with a phase shift. The actual synchronous signal of the converter has a phase shift θ owing to the delay of the sensor, delay of the IC, a way of a generating dead time, and so on. The load current I_L at $\theta = 0$ can be described by using d and T which is the period of I_O, as follows:

$$I_L = \frac{1}{\pi} \int_{-\frac{T}{2}}^{\frac{T}{2}} f_{conv}(I_O, d)dt. \tag{12}$$

Note that the function f_{conv} is a function of the load current I_O and Duty d. As shown in Fig. 3, d is used as arguments and switches between On and Off.

Described in section II-B, I_O is a sinusoidal wave and has no phase delay. Thus, Eq. (12) can be rewritten as follows, using the current path described in Fig. 4, and I_O current
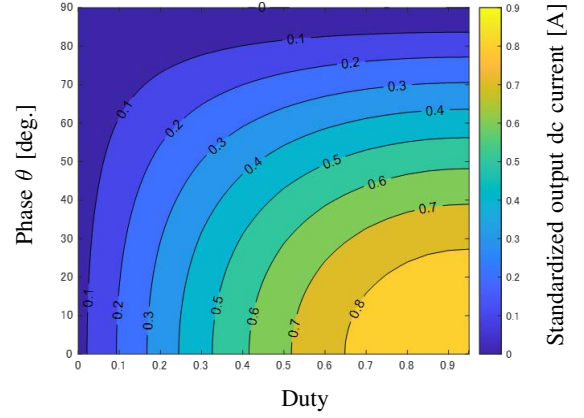

Fig. 6: Simulation results of how the dc current value changes when the ac current is 1 Arms, and the duty cycle and θ are changed shown in Fig. 5.
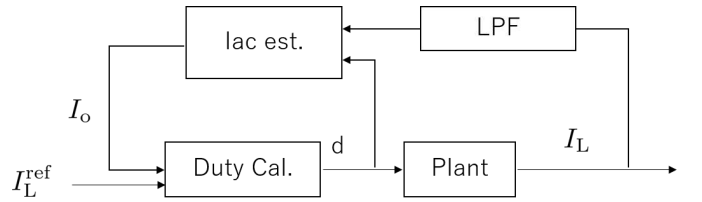

Fig. 7: Proposed estimation feed forward control method.

waveform of time in Fig. 5 which is a periodic function of T:

$$
\begin{aligned}
I_L &= \frac{\sqrt{2}I_{ac}}{2\pi}\left(\int_{-\frac{Td}{4}}^{\frac{Td}{4}} \cos\omega t dt - \int_{-\frac{T}{2}-\frac{Td}{4}}^{-\frac{T}{2}+\frac{Td}{4}} \cos\omega t\right). \\
&= \frac{\sqrt{2}I_{ac}}{2\pi}\left(\int_{-\frac{Td}{4}}^{\frac{Td}{4}} \cos\omega t dt + \int_{-\frac{Td}{4}}^{\frac{Td}{4}} \cos\omega t\right). \\
&= \frac{\sqrt{2}I_O}{\pi}\int_{-\frac{Td}{4}}^{\frac{Td}{4}} \cos\omega t dt. \\
&= \frac{2\sqrt{2}I_O}{\pi}\sin\frac{\pi d}{2}. \tag{13}
\end{aligned}
$$

The dc load current is expressed by Eq. (13) using the rms value of the ac coil current.

Fig. 6 shows the current value of I_L for varying θ and d expressed in Eq(13) when $I_O = 1$ A. As stated above, the phase difference θ is caused by the delay of the sensor and the ICs. the duty d is also assumed to vary from the generated the duty value because the gate signal is reduced due to the dead time. The current difference between $\theta = 0$ and θ=10deg. is about 1.5%, and for 20deg. the difference is about 9.4%. Note that 10deg. at 85 kHz is 327 ns, and for 20deg. is 654 ns. If the delay time of the sensor or IC can be kept within this time range, the current error is valid.

The delay time is also possible to compensate by calculating it in advance from the specification sheet of the IC and other components [16]. In the case of synchronous rectification operation near the duty $d = 1$, achieving perfect zero-cross switching of the voltage results in a larger power loss due
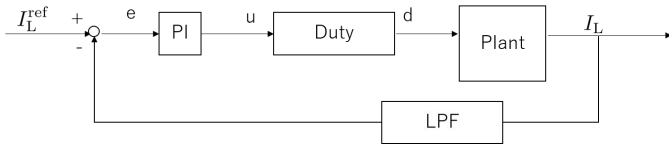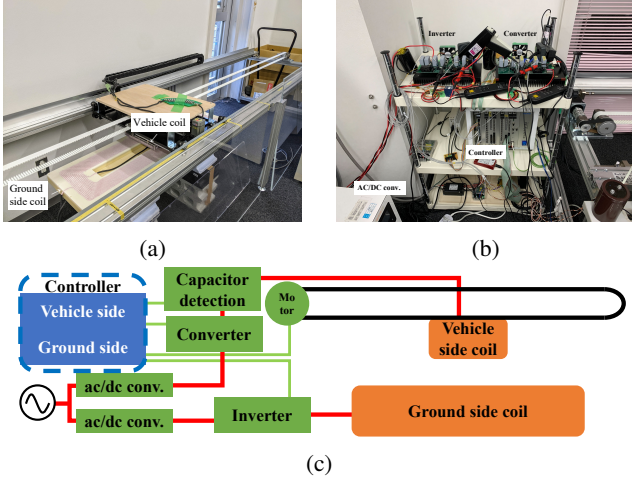
Fig. 8: PI block diagram.

Fig. 9: Experimental setups. (a)Experimental bench system of dynamic WPT coils. (b)The inverter, converter, and controller. (c)schematic diagram of Experimental setup.

to the longer commutation time [21]. Therefore, this paper intentionally does not compensate the dead time.

D. Proposed estimation method and current control

Fig. 7 shows the proposed current control method. The coil current I_O is estimated using the load current I_L obtained by the dc current sensor and the duty d which is previous output from the controller, note that the sample value of one previous sample of the sensor output is used. The duty is calculated using both the estimated ac coil current $\widehat{I_O}$ and the load current command value I_L^{ref}, the load current and the duty are the sensed current and command value of one previous sample is used. These values are denoted $I_L[z^{-1}]$ and $d[z^{-1}]$, respectively. $\widehat{I_O}$ is converted to the feed forward current control and is calculated in the following equation.

$$\widehat{I_O} = \frac{\pi}{2\sqrt{2}} \frac{I_L[z^{-1}]}{\sin\dfrac{\pi d[z^{-1}]}{2}}. \tag{14}$$

Note that θ illustrated in Fig. 5 is assuming zero. Also, the duty command is calculated by;

$$d^* = \frac{2}{\pi} \sin^{-1}\left(\frac{\pi}{2\sqrt{2}} \frac{I_L^{ref}}{\widehat{I_O}}\right). \tag{15}$$

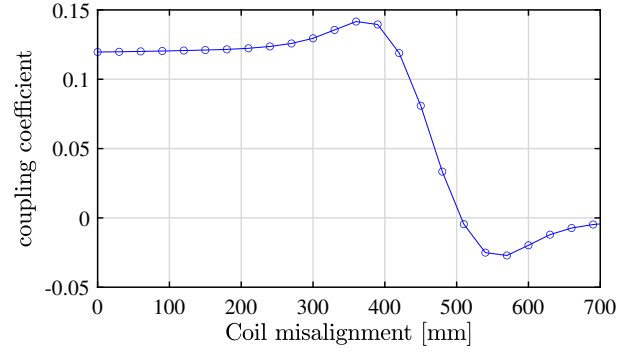Fig. 8 shows the PI block diagram for the comparison. A plant model is shown in Eq. (13). A small signal response of

Fig. 10: The coupling coefficient of misalignment to the x-direction(driving direction).

(a)

(b)
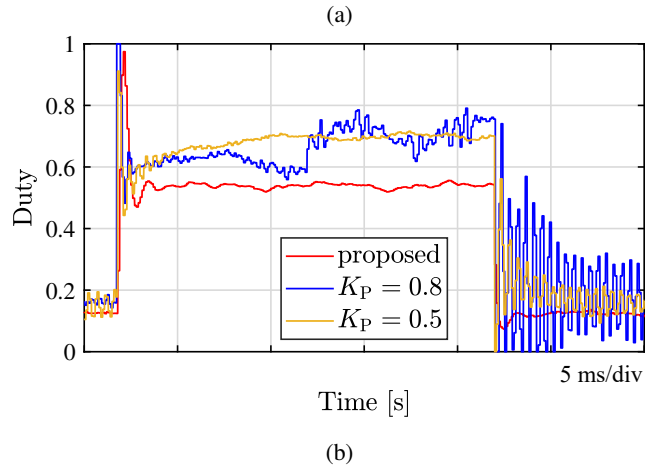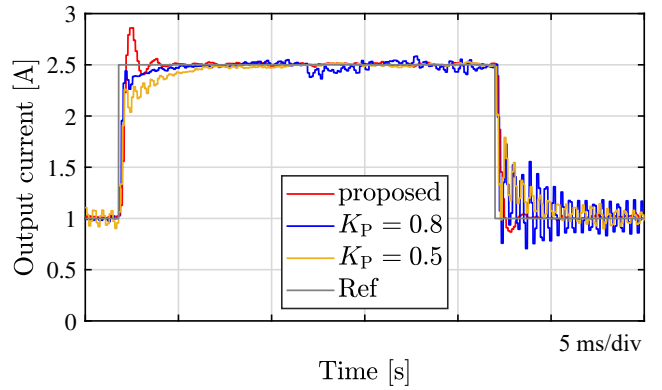
Fig. 11: Static response experimetal results (a) Current response of the static condition (b) Duty response of the static condition

the plant from the duty to I_L is described by the following equation, which value is the steady state values of $\bar{I_O}$, and $\bar{D}$.

$$G = \frac{\Delta I_L}{\Delta d} = 2\bar{I_O}\cos\frac{\pi\bar{D}}{2}. \tag{16}$$

Eq. (16) is not liner as the duty. The transfer function of this plant was used to determine the gain of the PI control, and the PI gain in this experiment was experimentally determined.

TABLE I: WPT Coil Parameters

L_P	244.2 μH	r_P	340.8 mΩ
L_S	100.6 μH	r_S	82.87 mΩ
C_P	14.23 nF	η_{max}	98.73
C_S	33.96 nF	R_{Omax}	7.63 Ω
LPF Cut-off frequency			1 kHz
Designed dead time			800 ns

III. EXPERIMENTAL RESULTS

A. Experimental parameters of the experimental system

Fig. 9 illustrates the experimental setup of this paper. The experimental system tested in this paper is shown in Fig. 9a. The bench system has one ground-side coil and is moving the vehicle coil at a constant speed in the driving direction. Owning to the servo motor's encoder counts, it enables precise position acquisition. For this experiment, the vehicle coil travel speed is set to 5.89 km/h. Fig. 9b shows the configuration of the power supply and its controller. SiC half-bridge modules are used for the inverter on the ground side and the converter on the vehicle side. The two converters are shown in the upper row of Fig. 9b. The controller is shown in the center and uses PE-Expert4. On the ground-side, MWPE4-PEV is used for over current control, which is implemented to stop power transmission when the ground side coil current exceeds 20 A. On the vehicle side, MWPE4-FPGA6 is used for the power receiving control. The synchronous signal sequence uses the algorithm shown in [16]. The calculation of the duty is also programmed in the FPGA displayed in Fig. 7. The AC/DC converters on the input and output sides use pCUBE and are shown in the lower left corner of Fig. 9b. Fig. 9c shows the schematic diagram of the experimental setup explained above.

In this experiment, the dc voltage on the ground side V_{DC} was kept constant. In addition, the vehicle-side voltage V_L was kept constant instead of a battery which ACDC converter was used to provide a constant voltage.

Table I shows the circuit parameters and control parameters for the experimental system. Fig. 10 described the coupling coefficient against the distance. The coupling coefficient remains $k = 0.12$ until $x = 200$ mm. The coupling coefficient increases as $x = 360$ mm, reaching a maximum value of $k = 0.142$. The coupling coefficient becomes negative at about $x = 500$ mm.

B. Experimental verification of static condition

The static experiments were conducted to verify the proposed control method in section II-D. The proposed method compares with a simple PI control shown in Fig. 8. The parameters of the experiment were shown in Table I. The input voltage V_{DC} and output voltage V_L were both set to 40 V respectively. The gain K_P is set to a range from 0.5 to 1.0. The time constant of the I gain was set to 1 ms which is the same as the time constant of the low pass filter shown in Fig. 8.

Fig. 11 describes the experimental results in the stationary state. The measured output current I_L of the PI control and the proposed method when the command value was changed
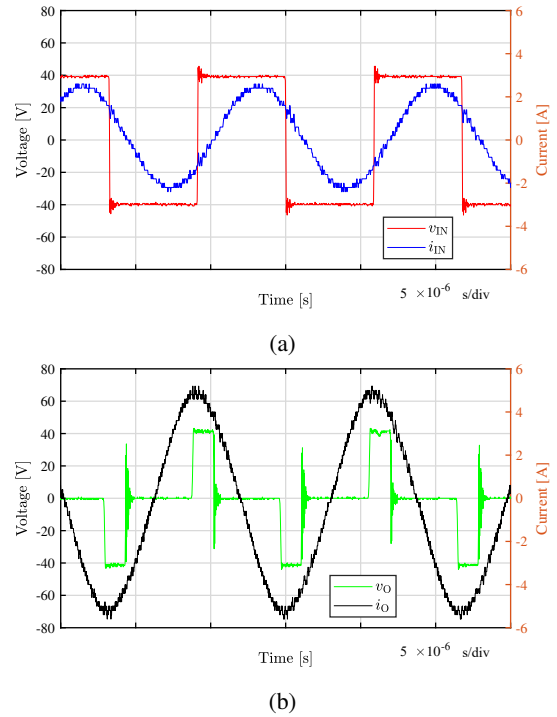

(a)

(b)

Fig. 12: Static experimental results of the WPT system at $I_L = 1$ A shown in Fig. 1 at $V_{DC} = V_L = 40$ V. (a) Waveforms of inverter output voltage v_{IN} and current i_{IN}. (b) Waveforms of converter input voltage v_O and current i_O.

from 1.0 A to 2.5 A and then to 1.0 A again. The response performance of the rising and falling edges of the PI control is very different. The duty of the PI control at $K_P = 0.8$ is fluctuating for not stable control. Also, the Duty at $K_P = 0.5$ is oscillated at falling state. PI control is difficult to judge that the current has converged completely.

This is owning to the nonlinearity of the plant, and the relationship between the duty and the load current which is defined by Eq. (13) as in the sinusoidal function. The Plant G is not a linear function with respect to the duty, as shown in Eq. (16). Since the load current value is controlled by a wide range in the proposed method, the duty varies widely between $0 < d < 1$. Therefore, G is not a constant value even when the sine function is linearized around the operating point. Consequently, the value of the transfer function differs between the rising and falling edges. For example, if the output current value $\bar{I}_L$ is small, $\bar{D}$ is a small value and G becomes a large value for cosine function. In contrast, if $\bar{I}_L$ is large, G is a small value. Even if the PI gain setting converges on the rising edge, it is not guaranteed to converge on the falling edge, because the Plant is not the same response as rising and falling state. Therefore, it is difficult to construct a feedback control using classical PI control in this method. The current values of the proposed method appear to overshoot at rising state, yet fast convergence of current values can be observed in the proposed method at the rising and falling states in Fig. 11. The proposed method and the PI control with $K_P = 0.5$ converged 3.1 ms and 5.2 ms on the rising state, respectively. Similarly,
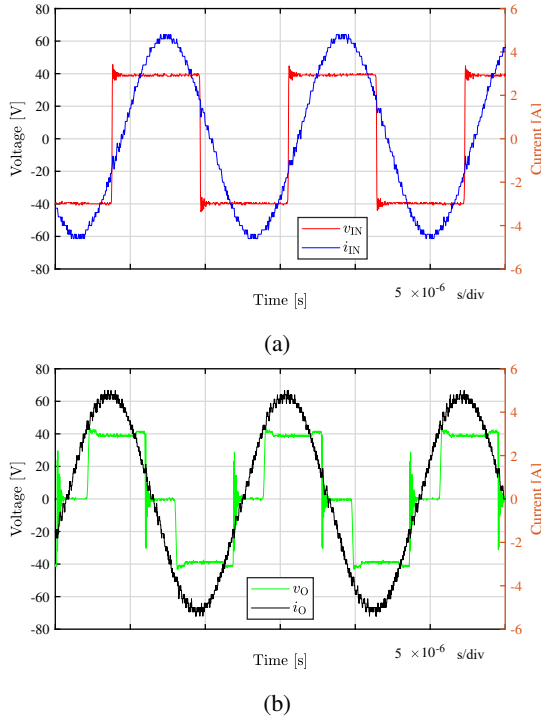
(a)

(b)

Fig. 13: Static experimental results of the WPT system at $I_{\mathrm{L}} = 2.5$ A shown in Fig. 1 at $V_{\mathrm{DC}} = V_{\mathrm{L}} = 40$ V. (a) Waveforms of inverter output voltage v_{IN} and current i_{IN}. (b) Waveforms of converter input voltage v_{O} and current i_{O}.

the convergence of the falling state was 1.8 ms and 5.5 ms. The proposed method was verified that Duty converges in a few ms.

Figs. 12, 13 shows the experimental waveforms of v_{IN}, i_{IN}, v_{O}, and i_{O}, in Fig. 1 at $I_{\mathrm{L}} =1.0$ and 2.5 A, respectively. Other experimental parameters and setup are the same as the previous experiment shown in Fig. 11. The operating frequency of the inverter is 85.5 kHz. Each waveform also shows a delay of the phase between v_{O} and i_{O} about 500 ns due to the delays of the sensor and ICs. The load current follows the command value very well even though the proposed feed forward control estimates the ac coil current. As discussed in Fig. 6, a phase difference of $\theta = 20$deg. shows a small deviation from the current at the difference of $\theta = 0$. The voltage increase during the dead time for the diode voltage is clearly observed in Fig. 13b. θ is 395.6 ns and 470.1 ns at $I_{\mathrm{L}} = 1.0$, 2.5 A. The phases between v_{IN} and i_{IN} are 31.7deg. and19.4deg. at $I_{\mathrm{L}} = 1.0$, 2.5 A, respectively. These phase errors are due to the difference of the vehicle-side resonant condition caused by the phase mismatch between V_{O} and I_{O}, which is affected by the dead time and delays of the circuit components. The currents i_{IN} and i_{O} are 1.84 Arms and 3.46 Arms in $I_{\mathrm{L}} =1.0$ A, 3.75 Arms and 3.68 Arms in $I_{\mathrm{L}} = 2.5$ A, respectively. The Duty commands are 0.128 and 0.535, respectively.

C. Experimental verifications of dynamic condition

1) Experimental result: Fig. 14 shows the results of the DWPT system using the bench system illustrated in Fig. 9a.
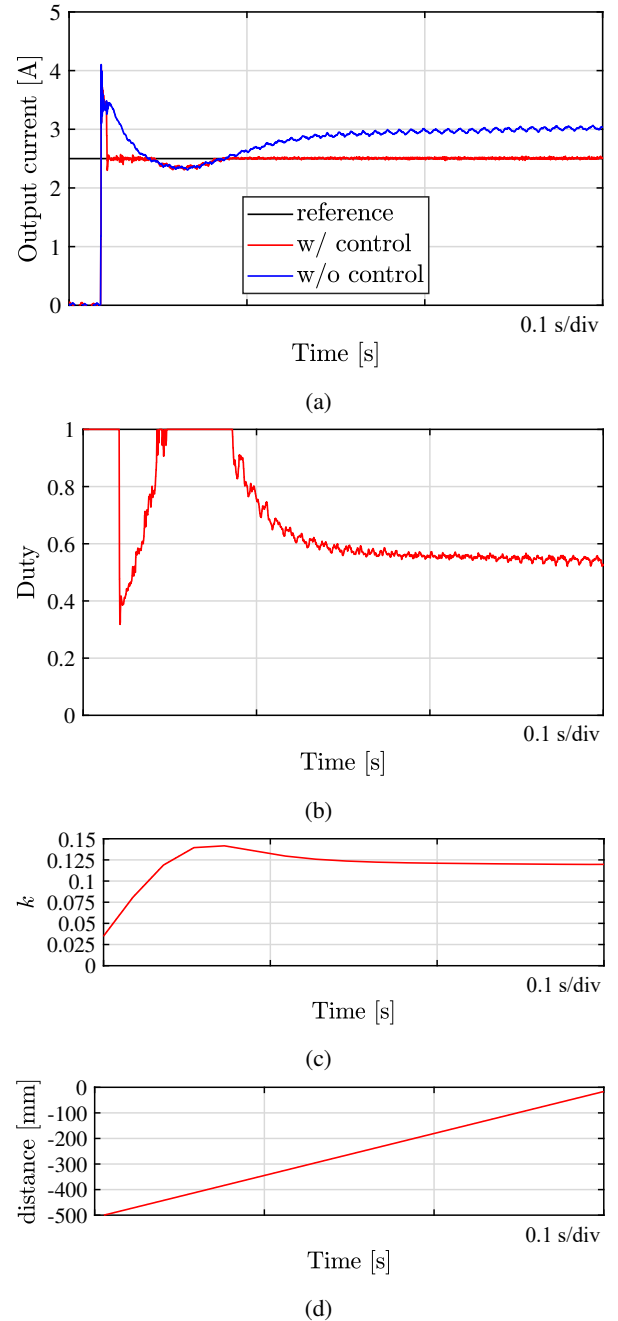

(a)

(b)

(c)

(d)

Fig. 14: Dynamic experimental results of the proposed WPT system using the bench system shown in Fig. 9a (a) Output current of the proposed method in synchronous rectification and $I_{\mathrm{L}} = 2.5$ A. (b) Output results of the culculated duty d in the proposed method. (c) The estimated coupling coefficient from calculated by Fig. 10 and the encoder information of the experimental setup. (d) The distance from the center of the ground-side coil to the center of the vehicle-side coil obtained by the motor encoder count.

In the DWPT system, the output current fluctuates due to the variation of coupling coefficient. The proposed method under the fluctuating condition is verified for the response instead of the current step command. Fig. 14c is the calculated results

of measured data of Fig. 10 and the results obtained from the encoder count. The input and output DC voltages V_{DC}, V_{L} are 40 V each. The power supply started at $k = 0.08$, which was obtained by the encoder count of the motor for bench move. The waveforms are compared by synchronous rectification which the duty is costant as $d = 1$. In other words, this condition under which the proposed method is not used. The synchronous waveforms are seen that the current value fluctuates as the coupling coefficient increases and decreases. The transmission start position could be implemented by using the ground-side inverter to estimate the coupling coefficient using a pulse voltage [22]. A significant current overshoot was observed immediately after the start of power transmission, but this is due to low coupling and a step response of the input voltage at the inverter. This current overshoot can be suppressed by methods such as predicting the ground-side voltage based on the equivalent fundamental WPT model and switching the converter on the vehicle side at the appropriate timing [14]. The decrease in the current of the proposed method around 0.45sec is due to the high coupling coefficient. Because the maximum duty is limited to one for not to exceed the switching period, shown in Fig. 14b. It is verified that the proposed estimation method is working well even to the coupling coefficient changing.

2) Vehicle speed affect: The faster the vehicle speed, the more it is affected by the proposed method. There is no additional effect of current with increasing speed. From the discussion of the vehicle speed in [8], the velocity effect is necessary at high speeds of 500 km/h, and does not need to be considered at speeds of 100 km/h for EV applications. Therefore, the variation of the current is determined solely by the coupling coefficient from Eq. (7). The coupling coefficient k varies the position of the vehicle coil shown in Fig. 10. The minimum distance of the variation k is 90 mm of which the power transfer range is from 0.08 to 0.142. The interval time of the variation k is 3.24 ms when the vehicle speed is at 100 km/h. Since I_{O} in this interval does not vary stepwise but almost linear, it might not be impossible to track I_{O} even with a settling time of 3.1 ms in the rising state in the proposed method. If the LPF frequency can be doubled to 2 kHz by using a high-performance current sensor or changing the sampling period in the FPGA, the converged time of the proposed method can be approximately halved, and the method can be adapted to a 100 km/h vehicle with sufficient margin.

IV. CONCLUSION

This paper has proposed a load current control method for a DWPT system only using vehicle-side assemblies to control the charging current for the vehicle condition. The system has been implemented the SiC MOSFET converter instead of the diode rectifier for the control. First of all, theoretical analysis of a series-series WPT system concludes that output ac current of the system was proportional to input ac voltage. Next, analysis of one PWM control derives that the small deviations of the pulse duty and the phase angle between the output ac voltage and current was not sensitive to the load current. The

deviations consist from the dead time of the converter and the delays of a sensor and a IC, respectively. The ac current estimation method has been proposed for feed forward control to the load current. The stationary WPT system has been tested to compare the proposed method and PI control. The proposed method has been confirmed to converge 1.1 ms and 3.7 ms faster than the PI control at rising and falling states, respectively. From the analysis, it has been demonstrated that the response of the PI control is different between the rising and falling edges because the output current model contains sinusoidal function of the duty command. It has been verified that the DWPT system is enable to follow the command value except when the coupling coefficient is high.

REFERENCES

[1] N. Shinohara and H. Matsumoto, "Experimental study of large rectenna array for microwave energy transmission," *IEEE Trans. Microw. Theory Tech.*, vol. 46, no. 3, pp. 261-268, Mar. 1998.

[2] Chwei-Sen Wang, O. H. Stielau and G. A. Covic, "Design considerations for a contactless electric vehicle battery charger," *IEEE Trans. Ind. Electron.*, vol. 52, no. 5, pp. 1308-1314, Oct. 2005.

[3] C. Song, H. Kim, Y. Kim, D. Kim, S. Jeong, Y. Cho, S. Lee, S. Ahn, J. Kim, "EMI Reduction Methods in Wireless Power Transfer System for Drone Electrical Charger Using Tightly Coupled Three-Phase Resonant Magnetic Field," *IEEE Trans. Ind. Electron.*, vol. 65, no. 9, pp. 6839-6849, Sept. 2018.

[4] Z. Yan, B. Song, Y. Zhang, K. Zhang, Z. Mao, Y. Hu, "A Rotation-Free Wireless Power Transfer System With Stable Output Power and Efficiency for Autonomous Underwater Vehicles," *IEEE Trans. Power Electron.*, vol. 34, no. 5, pp. 4005-4008, May 2019.

[5] A. Pacini, A. Costanzo, S. Aldhaher and P. D. Mitcheson, "Design of a position-independent end-to-end inductive WPT link for industrial dynamic systems," in *Proc. 2017 IEEE MTT-S International Microwave Symposium (IMS)*, 2017, pp. 1053-1056.

[6] A. Kurs, A. Karalis, R. Moffatt, J. D. Joannopoulos, P. Fisher, M. Soljacic, "Wireless power transfer via strongly coupled magnetic resonances," *Sicnece*, vol. 317, No. 5834, pp. 83-86, July 2007.

[7] J. Huh, S. W. Lee, W. Y. Lee, G. H. Cho, C. T. Rim, "Narrow-width inductive power transfer system for online electrical vehicles," *IEEE Trans. Power electron.*, vol. 26, no. 12, pp. 3666-3679, July 2011.

[8] T. Fujita, T. Yasuda, H. Akagi, "A Dynamic Wireless Power Transfer System Applicable to a Stationary System," *IEEE Trans. Ind. Appl.*, vol. 53, no. 4, pp. 3748-3757, July-Aug. 2017.

[9] M. Sato, G. Yamamoto, D. Gunji, T. Imura, H. Fujimoto, "Development of Wireless In-Wheel Motor Using Magnetic Resonance Coupling," *IEEE Trans. Power Electron.*, vol. 31, no. 7, pp. 5270-5278, July 2016.

[10] F. Lu, H. Zhang, H. Hofmann, C. C. Mi, "A Dynamic Charging System with Reduced Output Power Pulsation for Electric Vehicles," *IEEE Trans. Ind. Electron.*, vol. 63, no. 10, pp. 6580-6590. Oct. 2016

[11] B. J. Varghese, A. Kamineni, N. Roberts, M. Halling, D. J. Thrimawithana, R. A. Zane, "Design Considerations for 50 kW Dynamic Wireless Charging with Concrete-Embedded Coils," *Proc. 2020 IEEE PELS Workshop on Emerging Technologies: Wireless Power Transfer (WoW)*, pp. 40-44, Dec. 2020.

[12] F. Farajizadeh, D. M. Vilathgamuwa, D. Jovanovic, P. Jayathurathnage, G. Ledwich, and U. Madawala, "Expandable n-legged converter to drive closely spaced multitransmitter wireless power transfer systems for dynamic charging," *IEEE Trans. Power Electron.*, vol. 35, pp. 3794-3806, Apr. 2020.

[13] Z. Ma, M. Xiao, Y. Xiao, Z. Pang, H. V. Poor, B. Vucetic, "High-reliability and Low-Latency Wireless Communication for Internet of Things: Challenges, Fundamentals, and Enabling Technologies," *IEEE Internet Things J.*, vol. 6, no. 5, pp. 7946-7970, Oct. 2019.

[14] T. Hamada, D. Shirasaki, T. Fujita, H. Fujimoto, "Proposal of Sensorless Vehicle Detection Method for Start-up Current Control in Dynamic Wireless Power Transfer System," in *Proc. The 47th Annual Conference of the IEEE Industrial Electronics Society*, Toronto, Canada Oct. 2021.

[15] R. Mai, Y. Liu, Y. Li, P. Yue, G. Cao, Z. He, "An Active-Rectifier-Based Maximum Efficiency Tracking Method Using an Additional Measurement Coil for Wireless Power Transfer," *IEEE Trans. Power Electron.*, vol 33, no. 1, pp. 716-728, Jan. 2018.

[16] T. Fujita, S. Nagai, O. Shimizu, H. Fujimoto, Y. Ohmori, "Resonant Capacitor Voltage Based 85-kHz 3-kW Synchronous Rectification on Wireless Power Transfer System," in *Proc. 2022 Wireless Power Week (WPW)*, pp. 634-639, July 2022.

[17] S. Ann and B. K. Lee, "Analysis of Impedance Tuning Control and Synchronous Switching Technique for a Semibridgeless Active Rectifier in Inductive Power Transfer Systems for Electric Vehicles," *IEEE Trans. Power Electron.*, vol. 36, no. 8, pp. 8786-8798, Aug. 2021

[18] Z. Zhou, L. Zhang, Z. Liu, Q. Chen, R. Long, H. Su, "Model Predictive Control for the Receiving-Side DC-DC Converter of Dynamic Wireless Power Transfer," *IEEE Trans. Power Electron.*, vol. 35, no. 9, pp. 8985-8997, Sep. 2020,

[19] C. S. Wang, G. A. Covic, O. H. Stielau, "Power transfer capability and bifurcation phenomena of loosely coupled inductive power transfer systems," *IEEE Trans. Ind. Electron.*, vol. 51, no. 1, pp. 148-157, Feb. 2004.

[20] T. Yamanaka, Y. Kaneko, S. Abe, T. Yasuda, "10 kW contactless power transfer system for rapid charger of electric vehicle," in *Proc. EVS26*, pp. 1-9.

[21] Z. Zhang, H. Lu, D. J. Costinett, F. Wang, L. M. Tolbert and B. J. Blalock, "Model-Based Dead Time Optimization for Voltage-Source Converters Utilizing Silicon Carbide Semiconductors," in *IEEE Trans.Power Electron.*, vol. 32, no. 11, pp. 8833-8844, Nov. 2017.

[22] D. Shirasaki, H. Fujimoto, Y. Hori, "Sensorless Vehicle Detection Using Vehicle Side Voltage Pulses for In-motion WPT," in *Proc. IEEE PELS WoW*, Seoul, Korea (South), pp. 320-325, Nov. 2020

Toshiyuki Fujita received the B.S. degree in electrical engineering, the M.S. degree in physical electronics, and Ph.D degree in electrical and electronic engineering from the Tokyo Institute of Technology, Tokyo, Japan, in 2008, 2010, and 2017 respectively. Since 2014, he has been with Technova Inc., Tokyo. Previously, he was at Panasonic Corporation, Osaka, Japan from 2010 to 2014. In 2019, he joined the University of Tokyo, Chiba, Japan, as a project assistant professor. His research interests include WPT systems for electric vehicles, ac/dc converters, and its control methods. He is a member of IEE Japan, the Society of Automotive Engineers of Japan, and the Japan Society of Applied Physics.

Hiroshi Fujimoto received the Ph.D. degree in the Department of Electrical Engineering from the University of Tokyo in 2001. In 2001, he joined the Department of Electrical Engineering, Nagaoka University of Technology, Niigata, Japan, as a research associate. From 2002 to 2003, he was a visiting scholar in the School of Mechanical Engineering, Purdue University, U.S.A. In 2004, he joined the Department of Electrical and Computer Engineering, Yokohama National University, Yokohama, Japan, as a lecturer and he became an associate professor in 2005. He is currently an associate professor of the University of Tokyo since 2010. He received the Best Paper Awards from the IEEE Transactions on Industrial Electronics in 2001 and 2013, Isao Takahashi Power Electronics Award in 2010, Best Author Prize of SICE in 2010, the Nagamori Grand Award in 2016, and First Prize Paper Award IEEE Transactions on Power Electonics in 2016. His interests are in control engineering, motion control, nano-scale servo systems, electric vehicle control, motor drive, visual servoing, and wireless motors. He is a senior member of IEE of Japan,the Society of Instrument and Control Engineers, the Robotics Society of Japan, and the Society of Automotive Engineers of Japan. He is an associate editor of IEE of Japan Transactions on Industrial Application from 2013, and Transactions on SICE from 2013 to 2016. He is a chairperson of JSAE vehicle electrification committee from 2014.